Nonlinear electrodynamics of superconducting NbN and Nb thin films at microwave frequencies

C. C. Chin*
Department of Physics, Massachusetts Institute of Technology, Cambridge, Massachusetts 02139 and Rome Laboratory, USAF, Hanscom AFB, Massachusetts 01731

D. E. Oates
Lincoln Laboratory, Massachusetts Institute of Technology, Lexington, Massachusetts 02173

G. Dresselhaus
Francis Bitter National Magnet Laboratory, Massachusetts Institute of Technology, Cambridge, Massachusetts 02139 and Rome Laboratory, USAF, Hanscom AFB, Massachusetts 01731

M. S. Dresselhaus
Department of Electrical Engineering and Computer Science and Department of Physics, Massachusetts Institute of Technology, Cambridge, Massachusetts 02139
(Received 16 October 1991)

The surface resistance R_s of NbN and Nb thin films with particular reference to nonlinear effects is reported at high values of the microwave magnetic field $H_{rf} \leq 500$ Oe using a stripline resonator in the frequency range $0.6 \leq f \leq 12$ GHz. In the stripline geometry, the microwave current is concentrated on the narrow center conductor. Thus a high microwave current density and, therefore, a high H_{rf} can be achieved with moderate power. For Nb thin films, R_s does not increase with H_{rf} for low H_{rf} values, as expected from weak-link theory. However, for the NbN thin films, R_s at temperature T follows a $R_s(T,f) = R_{s0}(T,f) + S(T,f)H_{rf}$ dependence, for $f < 6$ GHz where $R_{s0}(T,f)$ is the surface resistance at zero H_{rf}, and the slope $S(T,f)$ is proportional to $f^{2.3}$. This nonlinear effect is consistent with Halbritter's weak-link theory. For $f > 6$ GHz, R_s shows a plateau in the dependence on H_{rf} the magnitude of which varies as $f^{3.5}$, which is not predicted theoretically. When H_{rf} increases above a critical value H_{rf}^c, the resonance curves for the stripline resonator become asymmetrical and the intermodulation products saturate, indicating strong nonlinearities. The temperature dependence of $H_{rf}^c(T)$ for Nb, in contrast to NbN, thin films follows that of the dc H_{c1}. Information on the granularity of NbN, derived from the present study, provides insights into the surface impedance of the granular high-T_c copper oxide thin films.

I. INTRODUCTION

The measurement of nonlinear electrodynamic effects in superconductors is of interest both for practical applications and for the study of the fundamental properties of the materials. In any practical electronic application, the designer must know how much power the conductors can handle and at which power level nonlinear effects such as harmonic generation and intermodulation (IM) distortion become appreciable. Therefore the magnitude and the detailed nature of the nonlinear effects must be measured and understood in order to facilitate widespread application of superconductors in microwave frequency electronics. Until recently, the principal application of superconductors at microwave frequencies was for particle accelerators,[1,2] and it is in this context that most of the previous work studying nonlinear effects was done. Our main interest is in the application of superconductors to analog microwave-frequency electronic devices, and therefore we have undertaken this study of nonlinear effects using thin films of Nb and NbN in the form of stripline resonators.

The nonlinear effects can also be used to study the fundamental properties of the superconducting materials. One of the sources of nonlinear electrodynamics in type-II superconductors can be vortex formation and motion, and thus measurements at microwave frequencies should yield information about the nature of pinning forces and the nucleation time of the vortices.

All materials show nonlinear effects in transport properties. In single crystals, the magnitude of the nonlinear effect is intimately associated with the crystal symmetry so that for materials with inversion symmetry, only odd harmonics would occur in the nonlinear excitations. For example, the first nonvanishing term in the nonlinear susceptibility for a material with inversion symmetry is $\chi^{(3)}$, since $\chi^{(2)}$ vanishes by symmetry.

The superconductors studied here show intrinsic nonlinear effects in the microwave region such as IM phenomena, where, for example, two frequencies f_1 and f_2 can be combined to give sum and difference frequencies. In addition to intrinsic effects, extrinsic nonlinear effects

associated with the sample morphology are sometimes observed. These are effects such as second harmonic generation or the other effects reported in this paper associated with the sample granularity.

Nonlinear effects in superconductors at microwave frequencies such as IM products,[4,9,10] power dependence of the surface impedance Z_s,[3,4] and a microwave critical field $H_{rf}^c < H_{c1}$, the lower critical field,[3,5–8] have been observed by many workers in a variety of materials. Although these investigations extend over many years, new interest in these nonlinear effects has been kindled since the discovery of the high-T_c oxide materials. Early experiments on the Z_s of the high-T_c materials also show a dependence on the incident microwave power,[11] and this work is currently being pursued.[12]

In previous papers we reported measurements of Z_s for NbN (Ref. 13) and Nb (Ref. 14) thin films by use of a stripline resonator at low H_{rf}. We found in Ref. 13 that the weak-coupling Mattis-Bardeen theory could be used to fit the temperature dependence of the surface impedance for a strong-coupling superconductor in the local and dirty limit as in the case of films of NbN. Table I summarizes the properties of the films reported in Refs. 13 and 14. In Table I, λ is the magnetic penetration depth, Δ is the energy gap, ξ_0 is the coherence length, ℓ is the electron mean free path, and T_c is determined at microwave frequencies.

In this work, we present results for Z_s of thin superconducting films of NbN and Nb at high values of the microwave magnetic field H_{rf} using a stripline resonator. From our measurements we find that the nonlinearity of Z_s has different character in two regions of H_{rf}: one of weak nonlinearity and one of strong nonlinearity. The region of weak nonlinearity is characterized by an increase in the surface resistance and the generation of IM products. In this region the resonance curves remain Lorentzian and symmetric about the center frequency. In the region of strong nonlinearity the resonance curves become asymmetric and show hysteresis and R_s increases sharply. Also the insertion loss increases and the IM products saturate. Often the strongly nonlinear regions exhibit a thermal instability.

NbN is of great interest because of its similarities to the high-T_c materials; for example, NbN is composed of oriented grains connected by weak links. Furthermore, NbN is strongly type II with a large upper critical field and a high critical current density. Also, the mechanism of superconductivity in NbN is well understood and all of the relevant BCS parameters have been measured. We also included Nb in the study because of the availability of high quality and well-characterized Nb films. Furthermore, the values of the Ginzburg-Landau constant κ are extremely different in NbN ($\kappa \gg 1$) and Nb ($\kappa \approx 2$). It is important to investigate how κ affects the nonlinear properties of type-II superconductors, especially the critical microwave magnetic field H_{rf}^c.

The surface resistance R_s of NbN increases on increasing the magnitude of H_{rf}. This effect is believed to be due to the granularity of the samples. Halbritter[15] has calculated the change of Z_s as a function of H_{rf} due to the high-frequency vortex penetration into the intergranular weak links. Comparison of the Z_s vs H_{rf} data of the

TABLE I. Film properties measured at microwave frequency and weak H_{rf} (Refs. 13 and 14).

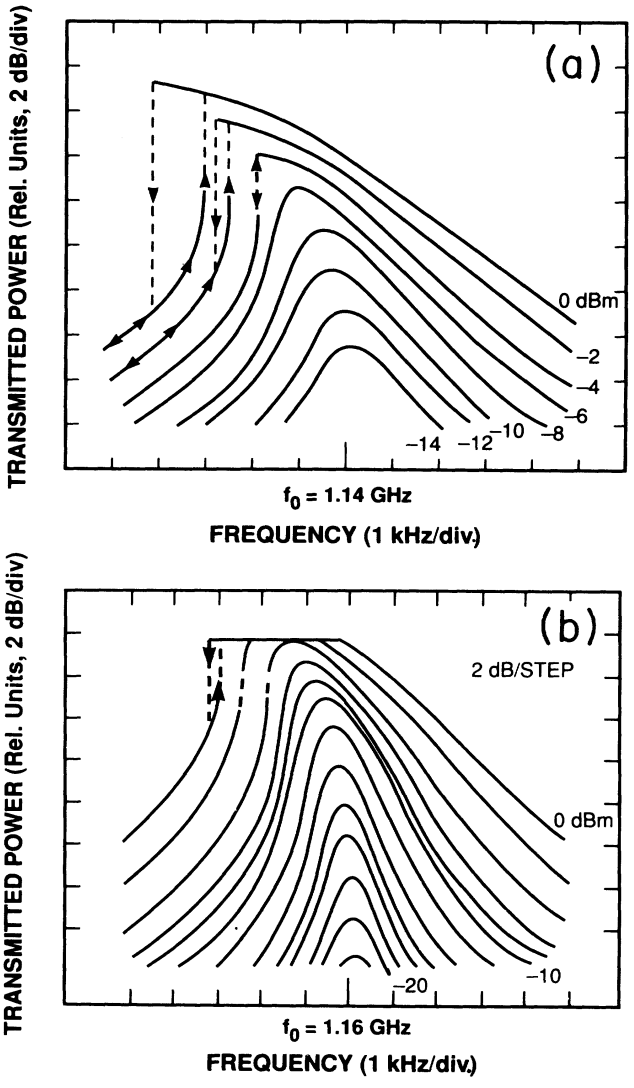

FIG. 1. (a) Line shape of the transmitted-power resonance curves of NbN at strong microwave magnetic field H_{rf}. Each curve is labeled by the power level. The asymmetry of the resonance curves at high power is shown, and these curves show hysteresis at an input power greater than −2 dBm.

granular NbN films with Halbritter's theory is of great interest and may provide important insights for the high-T_c data which also show a power dependence of Z_s.[12] In contrast, our Nb sample shows no power dependence of Z_s, perhaps because of different degrees of granularity and a low value of the nucleation frequency of the intergranular vortices. We will discuss the Nb data in more detail in Sec. III C 3.

When H_{rf} reaches a critical value H_{rf}^c, the resonance curves for the NbN and Nb resonators become asymmetric about the resonant frequency, with the peak resonant frequency shifted to lower frequency, as shown in Fig. 1(a) for NbN and 1(b) for Nb. H_{rf}^c will be defined more precisely in Sec. III C 2 where Fig. 1 is discussed further. The asymmetrical resonance curve has been observed by Hahn and Halama[1,2] on superconducting Nb using cavity measurements. Recent studies on high quality $YBa_2Cu_3O_{7-x}$ films by the stripline-resonator method show similar phenomena, and the data will be reported elsewhere.[16] Halbritter[17] has argued that the asymmetry of the resonance curve is caused by the power dependence of the surface reactance of the superconductor, which may be due to pair breaking, nucleation of high-frequency vortices, or other nonlinear effects. By measuring the temperature and frequency dependence of H_{rf}^c for both NbN and Nb, we are able to infer the physical reasons for the asymmetry of the resonance curves.

The outline of this paper is as follows: Section II discusses the sample preparation and stripline-resonator fabrication; Sec. III discusses the nonlinear surface impedance and gives results; Sec. IV discusses the intermodulation measurements and results; Sec. V discusses heating effects; and finally Sec. VI presents the conclusions.

II. SAMPLE PREPARATION AND STRIPLINE-RESONATOR FABRICATION

A. NbN and Nb film deposition

The NbN thin films used in this study were deposited on sapphire substrates by dc magnetron sputtering of a pure Nb target in an argon and nitrogen sputtering gas. The preparation method has been described in detail previously.[18] A film thickness of about 8000 Å was used in the stripline.

The Nb films were deposited on sapphire substrates by dc magnetron sputtering in an argon atmosphere. Immediately following the Nb deposition, ~30 Å of Al was deposited in the same system by dc magnetron sputtering and the system was back filled with O_2 to oxidize the Al film. The Al_2O_3 layer serves to passivate the Nb surface and prevents weak links from forming as the result of Nb oxidation.[19,20] The Nb film used in the stripline is 4000 Å thick. Our measurements of the dc properties of the NbN film are summarized in Table II. The results for the lower critical field H_{c1} were obtained using a superconducting quantum interference device (SQUID) magnetometer. The films of both materials are polycrystalline. The grain size was measured by transmission electron microscopy and in NbN is about 50 Å and in Nb about 1000 Å.

TABLE II. Film properties measured at low frequency and weak H_{rf}.

	T_c[a] (K)	J_c[b] (A/cm^2)	H_{c1}[c] (Oe)
NbN	15.8	2.5×10^6	350
Nb	9.2	1.3×10^6	1500

[a]Transition temperature as determined by dc transport measurements.

[b]Critical current as determined by dc transport measurements at 4.2 K.

[c]Lower critical field as determined by SQUID measurements at 4.2 K.

B. Stripline resonator

The stripline resonator is shown in Fig. 2. The stripline geometry is defined as having a center conductor symmetrically located between an upper and lower ground plane. The remaining space between the ground planes is filled with a dielectric. The resonator, seen most clearly in the top view of Fig. 2(b), consists of an isolated length of transmission line one-half wavelength long at the fundamental frequency. Overtone resonances occur at all multiples of the fundamental frequency. The resonator

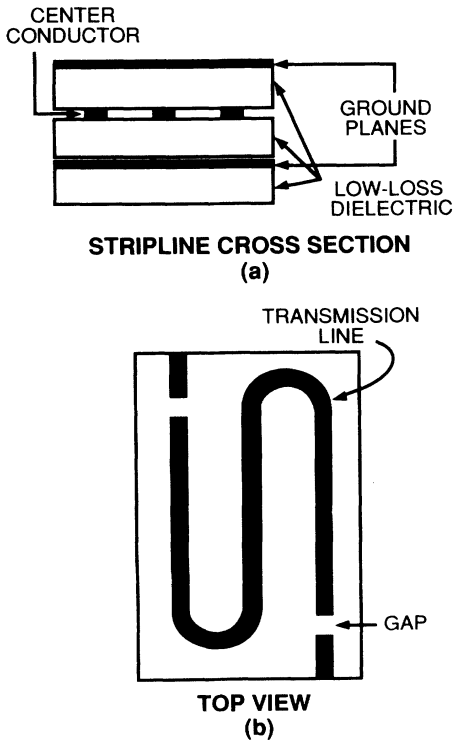

FIG. 2. Schematic diagram of the stripline resonator showing (a) the cross section and (b) the top view of the transmission line.

is capacitively coupled to the external circuit by gaps at the two ends of the stripline [see Fig. 2(b)]. In our case the length of line was chosen to yield a fundamental frequency of approximately 0.6 GHz. The conductor linewidth of 150 μm, fabricated on a 0.5-mm-thick sapphire dielectric substrate ($\epsilon = 10$), gives about 50 Ω for the transmission line impedance. The stripline was fabricated using standard photolithography and the NbN and Nb films were etched in a CF_4 plasma-etching system. The patterned transmission line with two ground planes of the same material is mounted in a gold-plated copper package with rf connectors mounted on the package. The stripline technique is ideal for carrying out surface impedance measurements in a strong H_{rf} field. Because the center conductor of the stripline resonator is very narrow and the resonator Q is high, a very low incident microwave power (of the order of 0.01 mW) can generate a strong H_{rf} field with a magnitude as high as ~300 Oe.

III. NONLINEAR SURFACE IMPEDANCE Z_s

A. Measurements of Z_s

The complex surface impedance $Z_s(T,f)$ can be written as

$$Z_s(T,f) = R_s(T,f) + iX_s(T,f), \tag{1}$$

where $R_s(T,f)$ and $X_s(T,f)$ are the surface resistance and the surface reactance, respectively. $X_s(T,f)$ can be written in terms of the magnetic penetration depth $\lambda(T)$ as $X_s(T,f) = \omega\mu_0\lambda(T)$. The stripline-resonator method of determining $R_s(T)$ and $\lambda(T)$ has been described in detail elsewhere,[11,13] and we give only a brief summary here.

To determine $\lambda(T)$ we measured the center frequency f_0 of the fundamental resonance as a function of temperature from low temperature (4.2 K) to T_c (or as close to T_c as possible). We then fitted $f_0(T)$ to a two-fluid or Mattis-Bardeen model expression for $\lambda(T)$ by using the calculated current distributions[14] to model the dependence of the stripline inductance on $\lambda(T)$.

To determine R_s, we find the Q of the resonator by measuring the 3-dB points of the transmitted-power-versus-frequency curve. The capacitive coupling gaps at the ends of the stripline are adjusted to yield a slightly under-coupled condition at resonance so that the measured Q and the unloaded Q_0 are almost equal. The Q is measured as a function of temperature and input power at the fundamental frequency of 0.6 GHz and at all of the overtone frequencies up to 12 GHz. The calculated current distribution, which depends on $t/\lambda(T)$ where t is the thickness of the film, is used to extract the surface resistance values from the measured Q. The details of this procedure are given in Ref. 14.

B. Determination of microwave magnetic field H_{rf}

The high Q values of the stripline resonator translate into very high current densities for the conductors. The method for calculating the rf current I_{rf} has been described in detail in Ref. 11. The total microwave current I_{rf} at the peaks of the standing waves at resonance is given by

$$I_{rf} = \sqrt{\frac{r_v(1-r_v)8Q_0P}{n\pi Z_0}}, \tag{2}$$

where r_v is related to the insertion loss L_I measured in dB by

$$L_I = -20\log_{10} r_v, \tag{3}$$

where Q_0 is the unloaded quality factor of the stripline resonator, P is the available incident power in units of W, n is the mode number of the resonance measured, and Z_0 (~50 Ω in this case) is the characteristic impedance of the transmission line.

The Q of the fundamental mode of the NbN and Nb resonators is high and is approximately equal to 2×10^6. Hence, input microwave power as low as −40 dBm can introduce a microwave current of the order of 3×10^{-2} A. Equation (2) gives the total rf current, but the distribution of current is not uniform. Sheen *et al.*[14] have calculated the microwave current density distribution $J_{rf}(x,y)$ for the geometry of the stripline as a function of λ. $J_{rf}(x,y)$, and therefore also H_{rf}, is found to be strongly peaked at the edges of the patterned stripline. In this paper, we use the results from Sheen *et al.*[14] to find the peak H_{rf} from the calculated I_{rf} peak in Eq. (2). In the following presentation of the data, H_{rf} always refers to the peak value at the edges of the stripline and at the peaks of the rf-standing-wave maxima.

C. Results for Z_s

1. Z_s vs H_{rf} for NbN

Figure 3 shows examples of the H_{rf} dependence of R_s of NbN for several low-order modes up to 6 GHz measured at 4.2 K, i.e., we plot R_s vs the peak H_{rf} at the edges of the transmission line. A few of the overtone resonance modes have low Q values and show a very weak dependence on temperature and power. The lowering of the Q results from coupling to low Q package resonances and these Q values therefore do not reflect the superconducting properties of the NbN and Nb. For this reason, as in a previous publication,[13] we have omitted these modes from the data presented and discussed. At low H_{rf} (< 30 Oe), the resonance curve is a Lorentzian and thus is symmetrical about the resonant frequency. When the incident power is increased to produce H_{rf} larger than about 30 Oe in NbN, the resonance curves become asymmetric and much wider, indicating a larger increase in R_s than that observed below 30 Oe. Figure 3 shows that, at low fields, R_s increases linearly with H_{rf} (or I_{rf}) and is given by

$$R_s(T,f) = R_{s0}(T,f) + S(T,f)H_{rf}, \tag{4}$$

where $S(T,f)$ is the slope of the linear increase and $R_{s0}(T,f)$ is the surface resistance at zero H_{rf}. Both S and R_{s0} are functions of frequency and temperature as

shown explicitly in Eq. (4). Figure 3 also shows that R_s vs H_{rf} is divided into two regions: one of weak nonlinearity at low fields, showing a linear increase in R_s, and one of strong nonlinearity at high fields in which R_s increases more sharply. The region of strong nonlinearity is discussed further in Sec. III C 2.

For $f < 6$ GHz all the modes show a similar linear dependence of R_s with H_{rf} at 4.2 K. We can get the value of $R_{s0}(4.2\text{ K}, f)$ by extrapolating the linear least-squares fit to $H_{rf} = 0$ for each of the f values measured. It was found that $R_{s0}(4.2\text{ K}, f)$ is proportional to f^2, the expected result.[13]

Above 6 GHz, a different feature appears. When H_{rf} reaches a certain value, a plateau in R_s (a region of nearly zero slope) is observed at all frequencies above 6 GHz and up to 10 GHz. Below the onset of the plateau $R_s(H_{rf})$ shows a linear increase with H_{rf}, as is also found in the lower-frequency modes. The resonance curve is still a Lorentzian both for H_{rf} values corresponding to the plateau region and below. Figure 4 shows an example of R_s vs H_{rf} measured at 6.89 GHz and 4.2 K, where the plateau can be clearly seen.

The modes exhibiting the plateau also enter a region of strong nonlinearity when H_{rf} is increased beyond the values shown in Fig. 4. The behavior is the same as for the lower-frequency modes, with asymmetric resonance curves and sharp increases in R_s with increasing H_{rf}. This is discussed further in Sec. III C 2.

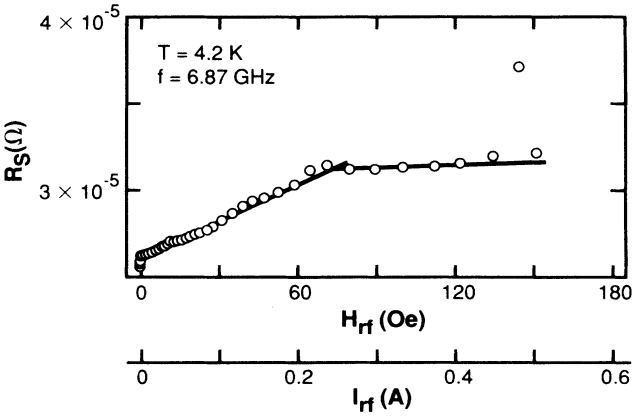

FIG. 4. Plot of R_s vs H_{rf} for NbN at 6.89 GHz and at 4.2 K. A plateau in R_s is observed for H_{rf} values above the regime of the linear increase of R_s with H_{rf}. Note the change of R_s scale from Fig. 3.

Figure 5 shows the data for the slope $S(4.2\text{ K}, f)$ vs f on a log-log scale obtained by a least-squares fit of Eq. (4) to the R_s data for $0.5 < f < 10$ GHz. Only the low-field, linear regions of Figs. 3 and 4 were included in the fit. By performing a least-squares fit to

$$S(4.2\text{ K}, f) = Af^{\nu} \tag{5}$$

the slope $S(4.2\text{ K}, f)$ was found to be proportional to $f^{2.3\pm0.3}$, as shown by the line in Fig. 5. Halbritter's weak-link theory[15] predicts an f^2 dependence of $S(T, f)$. Thus our result is consistent with Halbritter's theory (within experimental error) and with $R_s(H_{rf})$ resulting from flux penetration into the weak links between the grains.

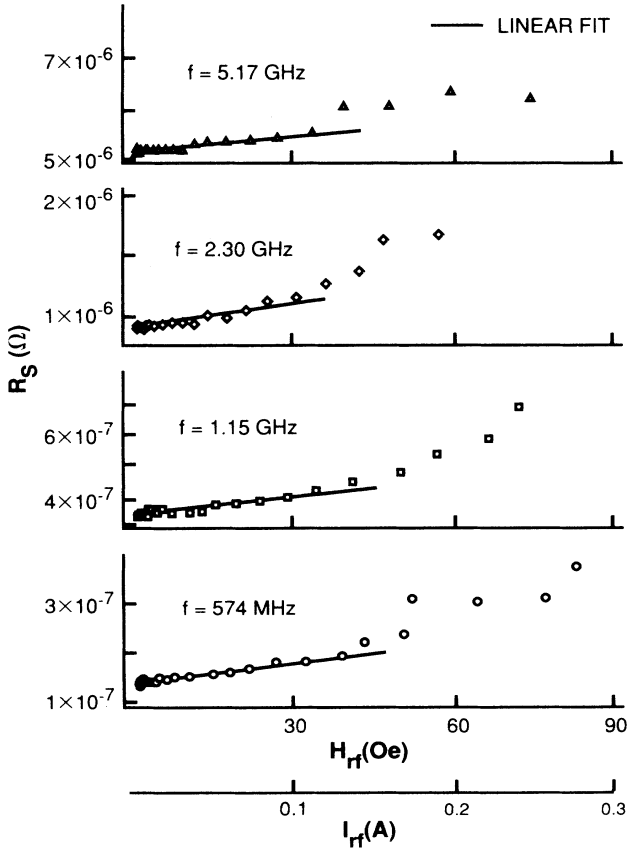

FIG. 3. Surface resistance R_s of NbN vs H_{rf} or I_{rf} measured at 4.2 K for different frequencies up to 6 GHz. Note the change of the R_s scale for the different frequencies.

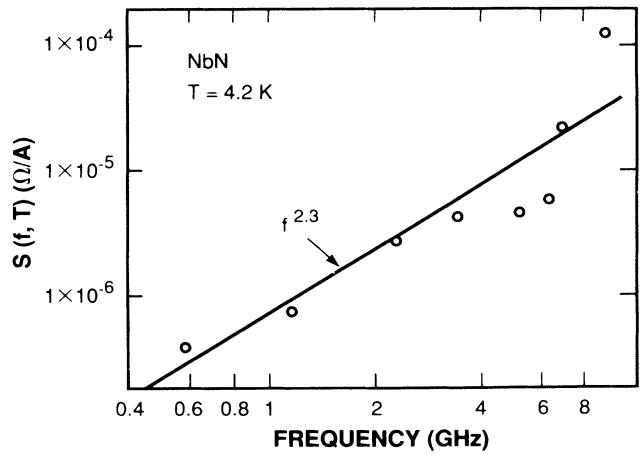

FIG. 5. Plot of the slope $S(T, f)$ of Eq. (4) vs f at $T = 4.2$ K. The points are experimental data and the line is a least-squares fit of the data yielding an $f^{2.3}$ dependence.

The value of the surface resistance of the plateau, R_{sat} at 4.2 K, for $6 < f < 10$ GHz was found to vary as $f^{3.5\pm0.5}$ by a least-squares fit of f^{ν} as is shown in Fig. 6. We have no explanation of either the existence of these plateaus or their frequency dependence shown in Fig. 6.

The temperature dependence of $S(T,f)$ was measured at 1.14 GHz, and the data are shown in Fig. 7. Also shown are two calculated curves derived from the following arguments. Halbritter's weak-link theory[15] shows that

$$S(T,f) \propto \frac{\lambda_J(T)}{H_{c2,J}(T)}, \tag{6}$$

where $\lambda_J(T)$ is the Josephson weak-link penetration depth, and $H_{c2,J}(T)$ is the upper critical field of the Josephson weak-link array formed by the grains of the sample. The weak-link penetration depth $\lambda_J(T)$ is given by

$$\lambda_J^2(T) = \frac{\hbar}{2\mu_0 e j_c(T)[2\lambda(T)+d]}, \tag{7}$$

where $j_c(T)$ is the critical current density, and d is the width of the Josephson junction of the weak link.

To fit the $S(T,f)$ data, we take $\lambda(0) = 3700$ Å $\gg d$,[13] where $d < 10$ Å. We also assume a two-fluid model temperature dependence expression for $\lambda(T)$. The macroscopic critical current measured by transport, $J_c(T)$, was found to vary as $1/[1-(T/T_c)^2]$. We assume that $j_c(T)$ has the same dependence on temperature as $J_c(T)$. Tinkham and Lobb[21] have modeled the upper critical field $H_{c2,J}$ of an array of Josephson junction weak links. Their model predicts no temperature dependence of $H_{c2,J}$. Figure 7 shows the comparison of the experimental data with Eq. (6) (dashed line) assuming that $H_{c2,J}$ is independent of temperature. There is a large discrepancy between the Tinkham and Lobb model and the experimental data in Fig. 7. A much better fit is obtained between the experimental data and Eq. (6) (solid line) by assuming

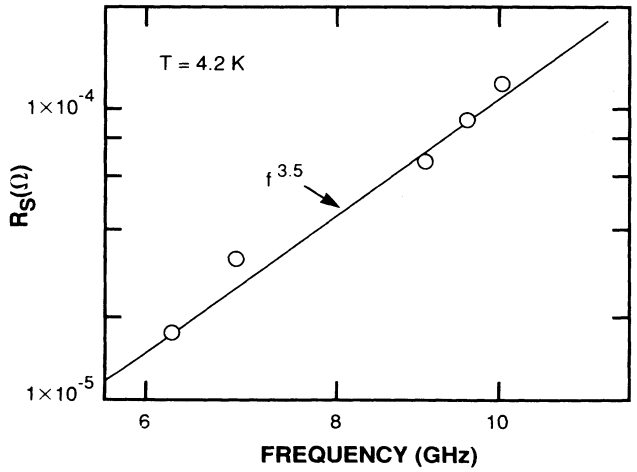

FIG. 6. Plot of surface resistance of the plateau R_{sat} vs f for NbN at 4.2 K. The solid line is a least-squares fit to the data yielding an $f^{3.5}$ dependence.

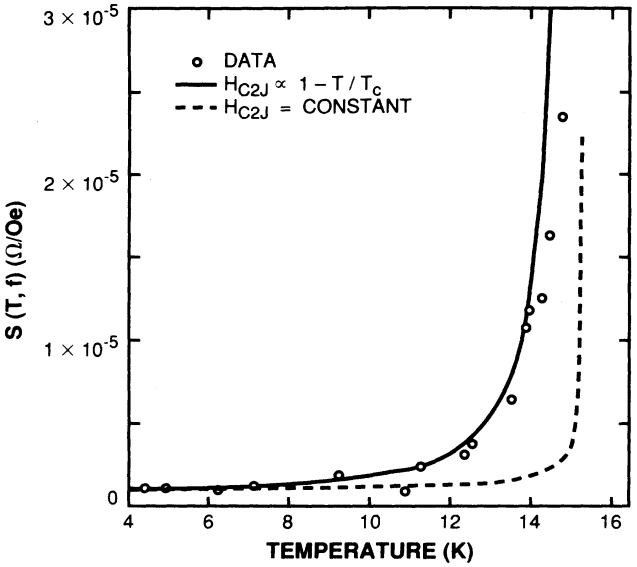

FIG. 7. Plot of the slope $S(T, 1.14\ \text{GHz})$ vs T compared with Halbritter's theory assuming a temperature dependence of $(1-T/T_c)$ for $H_{c2,J}$ (solid line) and of Tinkham's model (dashed line) for $H_{c2,J}$, independent of temperature.

$H_{c2,J} \propto (1-T/T_c)$.

In contrast to the behavior for R_s, we observe no change of $\lambda(4.2\ \text{K})$ for NbN on increasing H_{rf}. Halbritter's theory[15] predicts

$$\frac{\Delta\lambda}{\Delta R_s} \approx \frac{4\omega\mu_0 R_s^2}{3\lambda_J^2}, \tag{8}$$

where λ_J is the weak-link penetration depth, and is given by Eq. (7). By taking $R_s \approx 5\times10^{-7}\ \Omega$ at 1.14 GHz, $j_c \approx 2.5\times10^{10}$ A/m^2, and $\lambda \approx 3700$ Å at 4.2 K, we get $\Delta\lambda \approx 1\times10^{-7}$ Å, which is too small to be observed. Thus our experimental observations on X_s (i.e., $\Delta\lambda$) are also consistent with Halbritter's weak-link theory.

2. *Strong nonlinear effects and rf critical fields in NbN*

As mentioned above, when H_{rf} is increased beyond the linear R_s vs H_{rf} region, shown in Figs. 3 and 4, the resonance curve deviates from the Lorentzian shape observed at lower power and the line shape becomes asymmetric about the frequency of the maximum transmitted power f_{peak}. Figure 1 shows examples of resonance curves in this regime, such as for mode 2 at 1.14 GHz. Shown in Fig. 1(a) are a series of curves of transmitted power versus frequency for NbN where the input power is increased in 2-dB steps from −14 to 0 dBm. When the input power is greater than −4 dBm, the curves also exhibit hysteresis as shown. The shape of the curves resembles that calculated for a nonlinear harmonic oscillator.[17,22] The modeling of these curves will be published later.[16]

In order to quantify the transition from the symmetrical Lorentzian line shape to an asymmetrical line shape, we define the asymmetry parameter γ of the resonance curve as

$$\gamma = f_{\text{peak}} - (f_1 + f_2)/2, \tag{9}$$

where f_{peak} is the frequency at the peak of the resonance curve, and f_1 and f_2 are the frequencies at the -3-dB points on either side of the peak of the resonance curves. Figure 8 shows the plot of γ vs input power for the NbN resonator measured at 1.14 GHz and 4.2 K.

At low input power, γ is independent of input power and has a value of $\gamma \approx 70$ Hz, but at power levels greater than -16.5 dBm, γ is found to increase linearly with input power. The nonzero value of γ at low input power is due to a very small amount of rf coupling between the input and output ports of the resonator. The values of γ at high input power extrapolate to $\gamma = 0$ at -18 dBm. We define the critical rf magnetic field H_{rf}^c as that value of H_{rf} where γ extrapolates to zero on the linear plot (see Fig. 8). This definition of H_{rf}^c is somewhat arbitrary but gives a reasonable criterion for obtaining H_{rf}^c.

Although the resonance curve is no longer a Lorentzian when $H_{\text{rf}} \geq H_{\text{rf}}^c$, we find the Q of the cavity experimentally by measuring the 3-dB bandwidth of the curve. One must bear in mind that the surface resistance deduced by this method is only an approximate value. R_s thus defined increases rapidly when $H_{\text{rf}} > H_{\text{rf}}^c$.

It is interesting to note that H_{rf}^c can be defined alternatively by the H_{rf} field at which R_s increases and deviates from the linear fit to the low H_{rf} data. The corresponding critical input microwave power determined by such a criterion is -20 dBm compared with -18 dBm determined by the asymmetry criterion for NbN at 1.14 GHz. The values of H_{rf}^c and hence I_{rf}^c are independent of frequencies for $0.5 < f < 6$ GHz as indicated in Fig. 3 and borne out by the more precise $\gamma = 0$ criterion. At frequencies above 6 GHz, the value of H_{rf}^c is almost four times its value below 6 GHz. The increase in H_{rf}^c with frequency is associated with the observation of a plateau

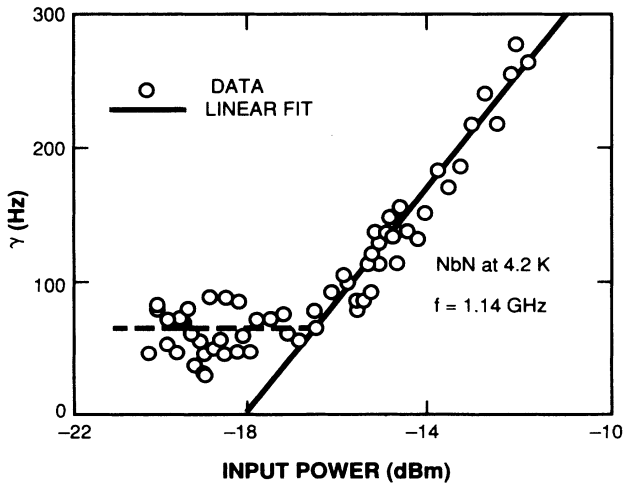

FIG. 8. Plot of the asymmetry parameter γ vs input power (see text). The small nonvanishing value of the residual γ at low input power is due to a very small amount of rf coupling between the input and output ports of the resonator. The value of γ at high input power extrapolates to zero at -18 dBm, which defines H_{rf}^c.

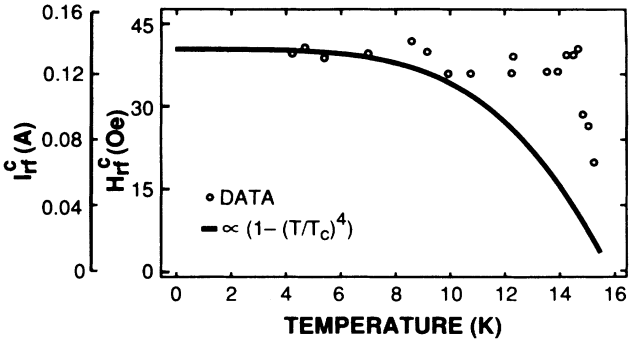

FIG. 9. The temperature dependence of $H_{\text{rf}}^c(T)$ and $I_{\text{rf}}^c(T)$ of NbN. The solid curve denotes a dependence proportional to $[1 - (T/T_c)^4]$ for reference.

in the surface resistance as a function of H_{rf} (see Fig. 4).

The temperature dependence of H_{rf}^c for NbN was measured at 1.14 GHz. The result is shown in Fig. 9. On the same graph, we plot (solid curve) the temperature dependence of the dc lower critical field $H_{c1}(T)$ given by the formula[23]

$$H_{c1}(T) = \frac{\Phi_0}{4\pi\mu_0\lambda^2(T)} \ln\kappa, \tag{10}$$

where Φ_0 is the magnetic flux quantum and κ is the Ginzburg-Landau parameter. Here $\lambda(T)$ is assumed to have a two-fluid model temperature dependence. $H_{c1}(T)$ is essentially proportional to $[1 - (T/T_c)^4]$, which is plotted in Fig. 9 and is shown just to illustrate its temperature dependence. A large discrepancy is found between the temperature dependence of $H_{\text{rf}}^c(T)$ and $H_{c1}(T)$ for NbN.

In order to see whether such a discrepancy is due to strong fluxoid pinning sites, the temperature dependence of the dc critical current J_c was measured and was found to vary as $1-(T/T_c)^2$, which rules out flux pinning as the explanation of the H_{rf}^c vs T curve. H_{c1} of the NbN thin film was measured by a SQUID at 4.8 K and was found to be in the range 350–500 Oe, which should be compared to the H_{rf}^c value of 40 Oe. Such a low H_{rf}^c may be due to the presence of weak links as well as regions of weakened superconducting properties in our NbN films. The weak regions allow enough flux penetration to increase the rf losses but not enough to influence the H_{c1} inferred from the magnetization curves measured in the SQUID.

3. Z_s vs H_{rf} for Nb

The R_s of Nb at 4.2 K does not depend on H_{rf} up to H_{rf}^c. Figure 10 shows R_s vs H_{rf} for several modes. For all points shown, the resonator curves are Lorentzian. Beyond the H_{rf} values shown in Fig. 10, H_{rf} exceeds H_{rf}^c, the resonance curve becomes asymmetric, and R_s increases rapidly. H_{rf}^c is found not to increase with frequency, as shown in Fig. 10. However, for $f > 6.3$ GHz, a substantial amount of power (> 1 W) is needed to exceed H_{rf}^c because of the lower Q values of the resonator

($Q_0 \propto 1/f$ for a superconductor). The higher dissipated power implies that we are observing some heating effects for $f > 6.3$ GHz as evidenced by a dependence of the resonance curves on the frequency sweep rate of the network analyzer at strong H_{rf}. Hence, we omit here the data on Nb for $f > 6.3$ GHz.

Similar to the measurements for NbN, the resonance curves of Nb become asymmetrical when $H_{rf} > H_{rf}^c$. In this connection, Fig. 1(b) shows examples of the resonance curves for mode 2 at 1.14 GHz for Nb. Shown are a series of curves of transmitted power versus frequency where the input power is increased in 2-dB steps from −24 to 0 dBm. The resonance curves start to become asymmetrical at −8 dBm. The curves for Nb are similar but not identical to those of NbN. Again, we observe hysteresis, which resembles that calculated for a nonlinearharmonic oscillator.[22]

The $H_{rf}^c(T)$ data for Nb are shown in Fig. 11. These results are found to follow the temperature dependence of $H_{c1}(T)$ of Eq. (10), which is also shown as the solid curve in Fig. 11. These results seem to indicate that we are measuring a critical-field quantity in Nb. However, $H_{rf}^c(4.8\ \text{K}) \approx 300$ Oe is smaller than $H_{c1}(4.8\ \text{K}) \approx 1500$ Oe. Halama[2] estimated 550 Oe for H_{rf}^c from cavity measurements on a large-grain-Nb cavity at 2.4 GHz and 1.4 K. Cavity measurements on differently prepared surfaces ranged from ~250 to 550 Oe. The difference between H_{c1} and H_{rf}^c is similar to that found for NbN. The reason for the difference between H_{c1} and H_{rf}^c is not known. The difference may arise from flux penetration in uniformly distributed, localized defects in the films which have lowered J_c. Further investigation of this difference is necessary to clarify the issue.

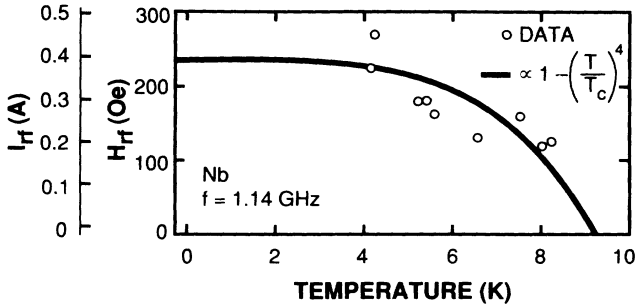

FIG. 11. Temperature dependence of $H_{rf}^c(T)$ and $I_{rf}^c(T)$ of Nb (open circles). The solid curve denotes a dependence proportional to $[1 - (T/T_c)^4]$ for reference.

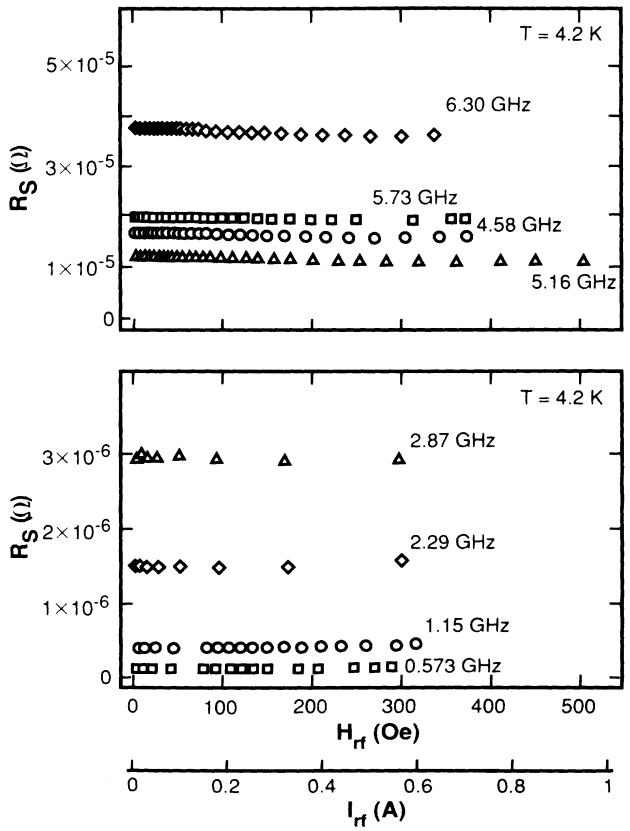

FIG. 10. Surface resistance of Nb vs H_{rf} or I_{rf} measured at 4.2 K for different frequencies. For H_{rf} greater than those shown, R_s increases sharply. These data points are not shown in the figure.

IV. INTERMODULATION PRODUCTS

A. Measurements

Nonlinear effects in superconducting materials lead to harmonic generation. Direct observation of harmonic generation in a stripline resonator is not possible because the resonant frequencies of the overtone modes are not exactly integer multiples of the fundamental frequency owing to a small amount of dispersion of the line. The nonlinearity responsible for harmonic generation can, however, be observed by intermodulation (IM) product measurements. In these measurements two signals of frequencies $f_1 = f_0 + \Delta f$ and $f_2 = f_0 - \Delta f$ from two synthesizers are combined and applied to the stripline resonator. Δf is chosen to be less than half of the 3-dB bandwidth. The IM products of frequencies $2f_1 - f_2$, $2f_2 - f_1$ (third-order IM), $3f_2 - 2f_1$, $3f_1 - 2f_2$ (fifth-order IM), etc., can be observed within the bandwidth of the mode by a spectrum analyzer. The measurements of the IM product were done at 4.2 K by immersing the stripline resonator into liquid helium to minimize heating effects. IM products are important in practical devices such as filters, but we have included IM measurements here because IM generation can only occur if the nonlinear effects are fast, i.e., a nonlinear response follows the microwave frequency with time constant $\tau < 10^{-10}$ s. Thermally generated nonlinear effects, for instance, will not produce IM products because of the much lower speed associated with thermal time constants ($\tau \geq 10^{-4}$ s). Thus our observation of IM generation confirms that the observed nonlinear Z_s behavior is due to true microwave-frequency nonlinearities and is not simply the result of heating even on a local scale.

B. IM results

The output power of the fundamental as well as that of the IM products versus the input power of the stripline resonator measured at 4.2 K and 1.14 GHz are shown in Fig. 12 (for NbN) and Fig. 13 (for Nb). Figures 12(b) and 13(b) also show for reference R_s vs power on the same scale. As expected, straight lines of slope 1, 3, and 5 can be fitted to the fundamental, third-, and fifth-order IM products, respectively. For both materials, the output power of the fundamental and IM signals saturates when the input power reaches a value which we call $P_{\rm sat}$. At $P_{\rm sat}$ the line shape of the resonance curves becomes asymmetrical, and thus $P_{\rm sat}$ corresponds (to within approximately ± 1 dB) to the power needed to produce $H_{\rm rf}^c$. It is found that the IM behavior is correlated with the behavior of $Z_s(H_{\rm rf})$. The saturation of the IM products is consistent with the sharp rise in R_s, which causes a large increase in the losses in the stripline thereby attenuating all signals, including the IM products. It should be noted that the third-order intercept, defined as the input power level at which the extrapolated third-order line intersects the first-order signal, is 20 dB lower for NbN than for Nb. Since the Q and insertion losses are similar, this indicates larger nonlinear effects occur in the IM products for NbN than for Nb, as is expected from the behavior of $R_s(H_{\rm rf})$ at low fields.

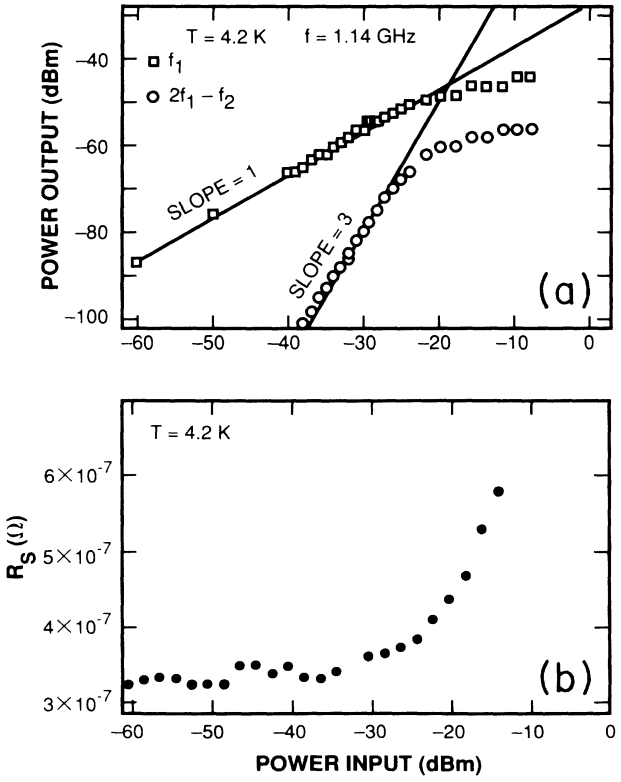

FIG. 12. (a) Power output of the IM signals vs power input for NbN measured at 1.14 GHz and $T = 4.2$ K; (b) surface resistance of NbN vs input power at 1.14 GHz and $T = 4.2$ K. Note that the power scales are identical.

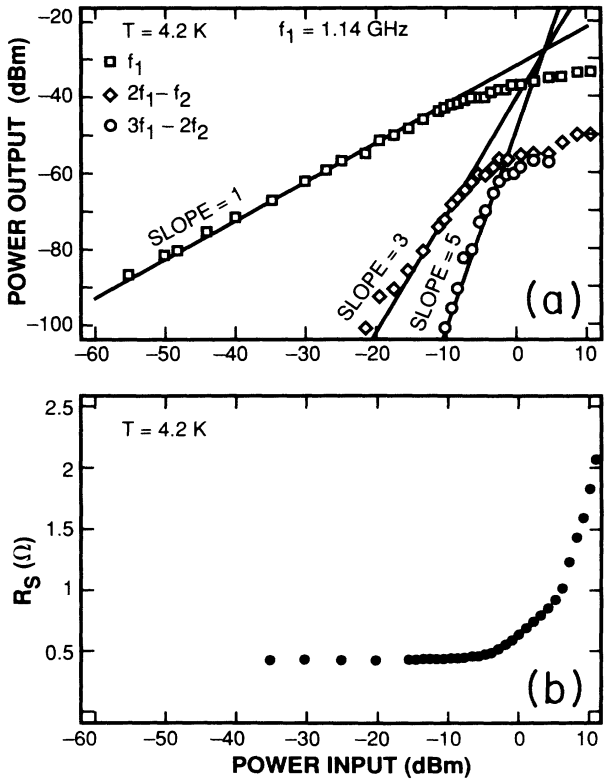

FIG. 13. (a) Power output of the IM signals vs power input for Nb measured at 1.14 GHz and $T = 4.2$ K; (b) surface resistance of Nb vs input power at 1.14 GHz and $T = 4.2$ K. Note that the power scales are identical.

V. INVESTIGATION OF HEATING EFFECTS

In the above, a number of nonlinear effects were reported as a function of $H_{\rm rf}$. As discussed in the previous section, the observed IM behavior rules out simple thermal effects as causing the nonlinear dependence of $R_s(H_{\rm rf})$ at low field. To investigate further the possibility of a thermal origin for the observation of these nonlinear effects, one mode of NbN was measured at high $H_{\rm rf}$ (i.e., the region of strong nonlinearity) and the measurement was then repeated with the input microwave power to the stripline resonator chopped by a rectangular amplitude modulation at 100%. In such an experiment we can introduce high $H_{\rm rf}$ fields but for a short time only, so that the amount of heat associated with the rf power could be controlled by the pulse length and repetition rate. The length of the microwave pulse was ~10 ms, and the repetition rate of the pulse was 1 Hz. The effective input power was thus reduced by a factor of 100. The length of the microwave pulse was chosen to be just long enough to build up steady-state microwave current in the high Q resonator. We find that the Q of the stripline resonator and the value of the microwave critical field $H_{\rm rf}^c$ remain unchanged with the chopped input signal. Even these measurements, however, do not completely rule out thermal effects with time constants less than 1 ms.

Further testing for heating effects was done by measuring H_{rf}^c and R_s while increasing H_{rf} for both NbN and Nb with the stripline resonator immersed first in the liquid helium and then in helium gas at 4.4 K. We could not measure any change in H_{rf}^c nor in the slope $S(T,f)$ of Eq. (4). These observations indicate that heating effects do not influence R_s at strong H_{rf} and are not responsible for transforming the resonance curve into an asymmetrical line shape.

VI. DISCUSSION AND CONCLUSIONS

We conclude from our measurements of the $R_s(H_{rf})$ that the nonlinearities may be divided into weak and strong regions. The weak nonlinear regimes in NbN show a linear increase in R_s with H_{rf}. In Nb, no increase in R_s is observed. The strong nonlinear regimes in both NbN and Nb are characterized by asymmetric resonance curves and sharp increases in $R_s(H_{rf})$, resembling critical behavior.

The linear increase of the R_s of NbN with H_{rf} is consistent with the granularity of the NbN films. The linear rise is associated with flux penetration in the intergranular material. The slope $S(T,f)$ varies as $f^{2.3\pm0.3}$ at $T = 4.2$ K, and this agrees within experimental error with the prediction of Halbritter's granularity theory[15] that $S(T,f) \propto f^2$. The R_s of the plateau (denoted by R_{sat}) varies as $f^{3.5}$. The physical reasons for the existence of the plateau and its variation with frequency are unknown. IM products were measured on the plateau region, and they followed the same slopes as in the nonplateau region. Thus, changes in the nature of the harmonic generation are not the cause of the plateau.

On the other hand, no increase of the R_s of Nb with H_{rf} is observed. The weak links of Nb are attributed to oxide-filled fissures caused by oxidation.[20] For niobium, $R_s \propto H_{rf}$ was obtained at 0.1 GHz by Piosczyk *et al.*[24] However, for $f > 0.5$ GHz, the increase of R_s was found to disappear with increasing H_{rf}.[15] This shows that the nucleation frequency of the vortices in Nb is ~ 0.5 GHz.[15] The Nb films are also granular, but the behavior of the links between the grains is different from that of NbN. Thus the intergranular material in Nb is not as weakened as that in NbN.

An important finding is that in both Nb and NbN H_{rf}^c, as measured and defined in this work, is significantly smaller than the dc H_{c1} that we have measured on samples fabricated by the same methods as those films used in the resonators. It is possible that H_{rf}^c is the field value at which flux penetration into the grains occurs. A detailed theoretical explanation of the lowered field H_{rf}^c does not exist yet. Halbritter has suggested[25] that the flux penetration takes place at microscopic defects and regions of "weakened superconductivity." This theory does not, however, explain why the dc H_{c1} is higher than the H_{rf}^c, nor does the theory explain the effects of the defects. If flux is penetrating into the grains, the effects should be seen in the magnetization curve. Perhaps the explanation lies in the fact that R_s measurements are more sensitive to the flux penetration at the defects than the dc measurements. R_s is very small to begin with; thus, changes in R_s are easily observed, while the dc measurements are just not sensitive enough. These questions are a matter that should be investigated further. An interesting observation here is that in Nb the H_{rf}^c can be related to the dc J_c we have measured. Using the I_{rf} value where H_{rf}^c is reached for Nb, we compute an average current density $J_{rf}^{ave} \approx 1.1 \times 10^6/\text{cm}^2$ which is very close to the dc J_c in Table I measured using the same stripline geometry as was used for the rf measurements. We have verified this relationship for two different widths of the stripline. For NbN, however, $J_c = 2.5 \times 10^6$ A/cm^2 and $I_{rf} = 1.0 \times 10^5$ A/cm^2. This difference in rf and dc J_c is consistent with the measurements of $H_{rf}^c(T)$, which indicates that in NbN the H_{rf}^c is not directly related to J_c.

When $H_{rf} > H_{rf}^c$, the resonance curves become asymmetrical. Figure 1 shows the resonance curves for NbN and Nb. These curves bear a close resemblance to those of a nonlinear oscillator, which can also show the hysteresis effects we have observed. We believe that a thorough analysis of the resonance curves using the concept of a nonlinear oscillator with nonlinear resistance and reactance can yield valuable information on the parameters of the superconducting thin films. For example, a fit to the data would possibly be capable of giving both $R_s(H_{rf})$ and $X_s(H_{rf})$ directly. Such an analysis is beyond the scope of this paper but will be presented in a future publication.[16]

For both NbN and Nb, H_{rf}^c is independent of frequency for $f < 6$ GHz. The antinodes of the resonant standing waves are at different positions on the center conductor for different modes. Hence, H_{rf}^c is not the consequence of the inhomogeneity of the sample.

The temperature dependence of $H_{rf}^c(T)$ or $I_{rf}^c(T)$ for NbN does not follow that of the dc $H_{c1}(T)$ (see Fig. 9). A similar effect was observed by Campisi[6] for Nb_3Sn using the cavity method. The temperature dependence of $H_{rf}^c(T)$ for Nb follows that of dc $H_{c1}(T)$. Recently, Shiren *et al.*[26] measured the temperature dependence of $\lambda(T)J_{rf}^c(T)$, the product of the penetration depth $\lambda(T)$ and the microwave critical current density J_{rf}^c of Nb at 16.5 GHz using a cavity method. The temperature dependence of $J_{rf}^c(\propto H_{rf}^c)$, deduced by Shiren *et al.* from the $\lambda(T)J_{rf}^c$ data by assuming a two-fluid model for the penetration depth $\lambda(T)$, also follows the dc $H_{c1}(T)$ for Nb. This result is consistent with our measurements on Nb.

In summary, we have shown that the nonlinear behavior of R_s of NbN at high power is consistent with Halbritter's weak-link model. Increases in R_s result from flux penetration at weak links which occur at grain boundaries. This nonlinear behavior has also been seen in granular films of the high-T_c oxide superconductors.[16] These results thus imply that it is necessary to employ single-crystal films which minimize grain boundaries and hence minimize R_s for high-power device applications.

ACKNOWLEDGMENTS

C.C.C. would like to acknowledge the hospitality of the MIT Lincoln Laboratory where all the experiments

reported in this paper were carried out. The research at MIT was supported in part by the Air Force Office of Scientific Research AFOSR-90-0123. The work at the Rome Laboratory was sponsored by the Department of the Air Force where G.D. was supported by the AFOSR University Research Resident Program. At the MIT Lincoln Laboratory the work was supported in part by the Department of the Air Force and in part by the Defense Advanced Research Projects Agency (Contract No. MDA972-90-C-0021) under the auspices of the Consortium for Superconducting Electronics. We acknowledge fruitful discussions with and suggestions by Dr. J. Halbritter concerning rf losses and flux penetration. He suggested the Al passivation of the Nb samples and also the application of nonlinear-oscillator theory. The authors wish to thank Dr. Alfredo Anderson for providing the NbN samples. We thank R.P. Konieczka for resonator fabrication, and W.T. Brogan and E.E. Macedo for sample preparation.

---

*Present address: Superconductivity Research Laboratory, 10-13, Shinonome 1-Chome, Koto-ku, Tokyo 135, Japan.

[1] H. Hahn and H.J. Halama, IEEE Trans. Nucl. Sci. **NS-16**, 1013 (1969).
[2] H.J. Halama, Part. Accel. **2**, 335 (1971).
[3] J.P. Turneaure, Ph.D. thesis, Stanford University, 1967; and (unpublished).
[4] R.V. D'Siello and S.J. Freedman, Appl. Phys. Lett. **9**, 323 (1966).
[5] T. Yogi, G. J. Dick, and J.E. Mercereau, Phys. Rev. Lett. **39**, 826 (1977).
[6] I. E. Campisi, IEEE Trans. Magn. **MAG-21**, 134 (1985).
[7] B. Hillenbrand, H. Martens, K. Schnitzke, and H. Diepers, in Proceedings of the 9th International Conference on High Energy Accelerators, Stanford Linear Accelerator Center, Stanford, California, 1974, p. 143.
[8] B. Hillenbrand, H. Martens, H. Pfister, K. Schnitzke, and G. Zeigler, IEEE Trans. Magn. **MAG-11**, 420 (1975).
[9] P. Bura, Appl. Phys. Lett. **8**, 155 (1966).
[10] A. S. Clorfeine, Appl. Phys. Lett. **4**, 131 (1964).
[11] D.E. Oates, A.C. Anderson, and P.M. Mankiewich, J. Superconduct. **3**, 251 (1990).
[12] D.E. Oates, A.C. Anderson, D. M. Sheen, and S. M. Ali, IEEE Trans. Microwave Theory Tech. **39**, 1522 (1991).
[13] D.E. Oates, A.C. Anderson, C.C. Chin, J.S. Derov, G. Dresselhaus, and M.S. Dresselhaus, Phys. Rev. B **43**, 7655 (1991).
[14] D. Sheen, S. Ali, D.E. Oates, K.A. Kong, and R.S. Withers, IEEE Trans. Appl. Superconduct. **1**, 108 (1991).
[15] J. Halbritter, J. Appl. Phys. **68**, 6315 (1990).
[16] P. Nguyen, D. Oates, C.C. Chin, G. Dresselhaus, and M.S. Dresselhaus (unpublished).
[17] J. Halbritter, J. Appl. Phys. **41**, 4581 (1970).
[18] A.C. Anderson, D.J. Lichtenwalner, and W.T. Brogan, IEEE Trans. Magn. **MAG-25**, 2084 (1989).
[19] J. Halbritter, J. Less Common Met. **139**, 133 (1987).
[20] J. Halbritter, Appl. Phys. A **43**, 1 (1987).
[21] M. Tinkham and C.J. Lobb, *Solid State Physics*, edited by H. Ehrenreich and D. Turnbull (Academic, New York, 1989), Vol. 42.
[22] C. Hayashi, *Nonlinear Oscillations in Physical Systems* (Princeton University, Princeton, NJ, 1985).
[23] T. Van Duzer and C.W. Turner, *Principles of Superconductive Devices and Circuits* (Elsevier, New York, 1981).
[24] B. Piosczyk, P. Kneisel, O. Stoltz, and J. Halbritter, IEEE Trans. Nucl. Sci. **NS-20**, 108 (1973).
[25] J. Halbritter (private communication).
[26] N.S. Shiren, R.B. Laibowitz, T.G. Kazyaka, and R.H. Koch, Phys. Rev. B **43**, 10 478 (1990).